Semiclassical description of wave packet revival

Fabricio Toscano[*]

Instituto de Física, Universidade Federal do Rio de Janeiro, CP 68528, 21941-972 Rio de Janeiro, RJ, Brazil

Raúl O. Vallejos[†]

Centro Brasileiro de Pesquisas Físicas (CBPF), Rua Dr. Xavier Sigaud 150, 22290-180 Rio de Janeiro, RJ, Brazil

Diego Wisniacki[‡]

Departamento de Física "J. J. Giambiagi," FCEN, UBA, Pabellón 1, Ciudad Universitaria, C1428EGA Buenos Aires, Argentina

We test the ability of semiclassical theory to describe quantitatively the revival of quantum wave packets—a long time phenomena—in the one dimensional quartic oscillator (a Kerr type Hamiltonian). Two semiclassical theories are considered: time-dependent WKB and Van Vleck propagation. We show that both approaches describe with impressive accuracy the autocorrelation function and wave function up to times longer than the revival time. Moreover, in the Van Vleck approach, we can show analytically that the range of agreement extends to arbitrary long times.

I. INTRODUCTION

From the early times of quantum theory there has been a lot of interest in the possibility of describing quantum phenomena using approximate theories that take advantage of classical information [1,2]. Not only because these *semiclassical* approaches provide in general a deeper insight into the system's behavior, due to the fact that classical quantities are more intuitive, but also in some cases the semiclassical computation of quantum quantities is made easier.

The semiclassical propagation of wave functions started with the seminal work of Van Vleck [3], where a semiclassical propagator was first introduced. Gutzwiller [4] showed that this propagator is the stationary-phase approximation of the Feymnan path integral, which results in a sum over classical paths. At the same time Gutzwiller provided some corrections to Van Vleck's formula which are essential for long times.

The propagation of wave functions using the Van Vleck-Gutzwiller propagator has fundamental problems that manifest themselves more sharply in systems with a classically chaotic dynamics. The facts that, for long times, the integrations to be performed are usually highly oscillatory, and therefore not amenable to numerical computation [2], and that the number of orbits becomes unmanageably large, has raised doubts about the long-time semiclassical accuracy. These problems were controlled in Ref. [5], where a semiclassical method was applied to compute autocorrelation functions of Gaussian wave packets. This approach was shown to work both for chaotic [5] and regular systems [6,7] in long-time regimes but it has not been applied to calculate wave functions.

More recently, in Ref. [8] it was shown that Gaussian wave packets can also be propagated by using the standard time-dependent WKB theory (TDWKB) [9], provided it is complemented with short-time methods. In principle this scheme is suitable to compute wave functions in the long-time regime. Although initially conceived for chaotic systems, the scheme also works for nonlinear integrable dynamics (see Sec. IV below).

Among the semiclassical time-domain methods one should also highlight the "initial value representation" (IVR) of the propagator, especially suited for numerical implementations (see Ref. [10] for a review).

In spite of the great advances in semiclassical theories in the last decades, there are still important open questions concerning the range of validity of semiclassical approximations and their accuracy in the description of subtle interference quantum effects such as, for example, quantum revivals.

The phenomenon of quantum revivals has been vastly studied in the literature (see Ref. [11] for a review) and observed in many experiments, from atomic and molecular to optical systems [12]. The Wigner function of an initially well-localized wave packet spreads for short times in a classical way, then it enters a delocalized quantum regime, and eventually it recombines itself to recover its original form. Such a revival occurs at a time, T_{rev}, which is long as compared with classical time scales such as oscillation periods. Perhaps more interestingly, in a wide class of circumstances, at times equal to a fraction of the revival time (pT_{rev}/q) the wave packet relocalizes into a number of smaller copies of the initial packet, giving rise to "fractional revivals." When the initial wave packet can be associated to an essentially classical state, the "fractional revival" occurrence corresponds to a dynamical generation of Schrödinger's catlike states (a quantum superposition of macroscopically distinguishable states).

One of the most interesting systems exhibiting both full and fractional revivals is the quartic oscillator, whose Hamiltonian is obtained by the squaring the harmonic oscillator Hamiltonian. In essence this is the Hamiltonian of the Kerr model, describing a single mode of the quantized radiation field in a nonlinear medium, and extensively studied in quan-

———————
[*]toscano@if.ufrj.br
[†]vallejos@cbpf.br; http://www.cbpf.br/~vallejos
[‡]wisniacki@df.uba.ar

tum optics. The formation of revivals and fractional revivals in this system was analyzed, for example, in [13]. Recently the quartic oscillator has experienced a renewed interest for its connections with quantum information processing in continuous variable (CV) systems. Indeed, Hamiltonians of the Kerr type are the simplest nonlinear ones acting on a single mode (i.e., one-mode quantum logic gate) needed to define universal quantum computation within the subclass of unitary transformations generated by Hamiltonians that are polynomial functions of the CV operators [14].

In addition to the already mentioned studies of revivals in the Coulomb problem [6,7], we must also mention the papers by Wang and Heller [15] and by Novaes [16]. The first authors considered the revival of a wave packet in the Morse potential. Using a convenient numerical implementation of the Van Vleck-Gutzwiller propagator they succeeded in reproducing satisfactorily the first revival of the wave function. Novaes studied the semiclassical propagation of a wave packet in the quartic oscillator, starting from the semiclassical coherent-state representation of the propagator. Even though he also obtained an excellent agreement, the increasing difficulty in determining the required complex trajectories as time grows limited the application of the method to short times (a few classical periods) [16].

The present paper is devoted to show that "elementary" semiclassical theories can be successfully applied to describe the revival phenomena in the quartic oscillator. Our study focus both on the autocorrelation function and on the wave function. The two elementary semiclassical theories examined are two: Van Vleck propagation (Sec. III) and time-dependent WKB (Sec. IV). In the first case, calculations are analytical; in the second, numerical. In both cases we find an excellent agreement between semiclassical theory and exact propagation even at very long times (e.g., multiples of the revival time). In the particular case of the Van Vleck autocorrelation function we show analytically that it agrees with the exact one up to arbitrary long times, the error being semiclassically small and independent of time. As a byproduct of our study, we show that TDWKB also works efficiently in integrable nonlinear systems [8].

Section II contains a description of the main aspects of the model. We present our main conclusions in Sec. V.

II. THE MODEL

Consider a one degree of freedom harmonic oscillator:

$$H = \frac{\hat{p}^2}{2m} + \frac{1}{2}m\omega^2\hat{q}^2. \tag{1}$$

Throughout the paper we set $m=1$ and $\omega=1$ (if desired, these constants can be recovered at any moment by dimensional considerations). We shall be interested in the dynamics of coherent states of this harmonic oscillator, i.e., eigenstates of the annihilation operator [17]

$$\hat{a} = \frac{1}{\sqrt{2\hbar}}(\hat{q} + i\hat{p}), \tag{2}$$

with $[\hat{a},\hat{a}^\dagger]=1$ ($\hat{a}^\dagger$ the creation operator). Our model to study the revivals and fractional revivals is the quartic Hamiltonian given by

$$\hat{H} = \gamma\hbar^2\left(\hat{a}^\dagger\hat{a} + \frac{1}{2}\right)^2 \equiv \gamma\hbar^2\left(\hat{n} + \frac{1}{2}\right)^2, \tag{3}$$

where $\hat{n}=\hat{a}^\dagger\hat{a}$ is the number operator. This nonlinear Hamiltonian is of the Kerr type [18]. Recall that the effective Hamiltonian that describes the dynamics of a single light mode inside a high finesse optical cavity containing a Kerr medium is

$$\hat{H} = \omega_1\hat{n}^2 - \omega_1'\hat{n} \tag{4}$$

(ω_1 and ω_1' are real frequencies), and we recover the optical context in our formalism considering $\hbar=1$.

The quantum evolution of a coherent state, $|\alpha_0\rangle$, with Hamiltonian (3) yields

$$|\psi\rangle = e^{-i\hat{H}t/\hbar}|\alpha_0\rangle = e^{-|\alpha_0|^2/2}\sum_{n=0}^{\infty}\frac{|\alpha_0|^{2n}}{\sqrt{n!}}e^{-i\gamma\hbar(n+1/2)^2 t}|n\rangle, \tag{5}$$

where $|n\rangle$ is a number state, i.e., $\hat{n}|n\rangle=n|n\rangle$. At multiples of the revival time

$$T_2 = \frac{\pi}{\gamma\hbar}, \tag{6}$$

the dynamics reconstructs the initial coherent state. For times equal to $(p/q)T_2$ (p/q an irreducible fraction) the evolved state consists of a superposition of q coherent states lying on a circle of radius $|\alpha_0|$ (fractional revivals) [13]. In Fig. 1 we show the Wigner function [19] of the evolved state (5) at several selected times. Schrödinger catlike states can be clearly seen at the fractional revival times.

We shall focus on the autocorrelation function,

$$C_1(t) = \langle\alpha_0|e^{-i\hat{H}t/\hbar}|\alpha_0\rangle = e^{-|\alpha_0|^2}\sum_{n=0}^{\infty}\frac{|\alpha_0|^{2n}}{n!}e^{-i\gamma\hbar(n+1/2)^2 t}, \tag{7}$$

in the semiclassical regime, defined by the condition $|\alpha_0|^2 \gg 1$, which is the appropriate semiclassical limit in the case of an optical context. It is important to note that this function shows the periodicity property

$$C_1(t + T_2) = e^{-i\pi/4}C_1(t), \tag{8}$$

the period being the revival time (6).

Note that the Weyl-Wigner representation [19,20] of Hamiltonian (3) is $\gamma[(q^2+p^2)/2]^2-\hbar^2/4$. Thus, the classical Hamiltonian corresponds to

$$H(q,p) = \gamma I^2, \tag{9}$$

with the action variable

$$I(q,p) = \frac{1}{2\pi}\oint p\,dq = \frac{1}{2}(q^2 + p^2), \tag{10}$$

a constant of motion.

III. VAN VLECK APPROACH

The semiclassical calculations in this section are based on the Van Vleck-Gutzwiller approximation [3,4] to the propagator:
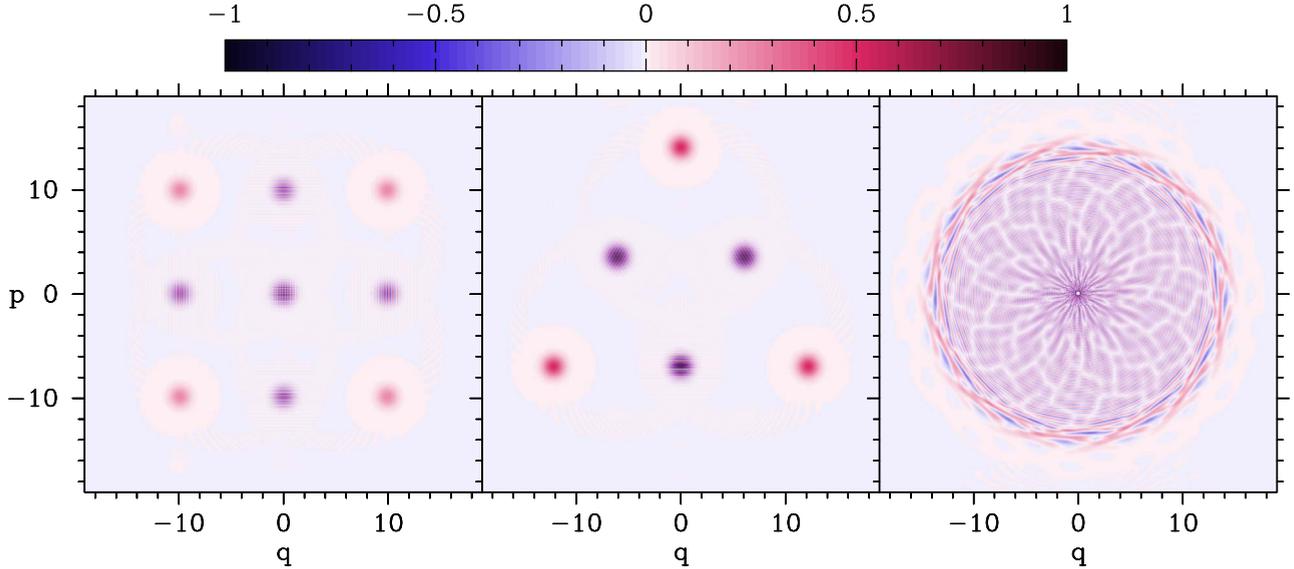
FIG. 1. (Color online) Snapshots of the evolution of an initially Gaussian wave packet (Wigner functions). From left to right, times are $t = T_2/4$, $T_2/3$, $T_2/2.385\,67$, with T_2 the revival time. The initial coherent state is centered at $(q_0, p_0) = (0, 14)$.

$$K(q'', q', t) \approx \frac{e^{-i\pi/4}}{\sqrt{2\pi\hbar}} \sum_k A_k e^{iS_k(q'', q', t)/\hbar - i\mu_k \pi/2}. \quad (11)$$

The sum runs over classical trajectories connecting q' to q'' in time t. Each trajectory contributes with an amplitude A_k and a phase. The phase is made up from the Lagrangian action S_k,

$$S_k(q'', q', t) = \int_0^t (p\dot{q} - H)dt, \quad (12)$$

and the Maslov index μ_k, which (in the present case) coincides with the number of turning points (where $\dot{q} = 0$) encountered by the trajectory [9]. The amplitude is given by

$$A_k = \frac{1}{\sqrt{|\partial q''/\partial p'|_k}}, \quad (13)$$

with

$$q'' = q''(q', p', t). \quad (14)$$

Equation (11) can be derived, for instance, by using time-dependent WKB theory to propagate a position eigenstate [9].

A. Autocorrelation function

Consider the autocorrelation function

$$C_2(t) = \int_{-\infty}^{\infty} \int_{-\infty}^{\infty} dq'' dq' \, \psi_0^*(q'') \psi_0(q') K(q'', q', t), \quad (15)$$

where $\psi_0(q)$ is the wave function of the initial state. By substituting the exact propagator $K(q'', q', t)$ by Van Vleck's we obtain a semiclassical correlation function.

The simplicity of the system we are considering permits the analytical determination of the required trajectories; the

properties of the trajectories can thus be calculated to the desired precision. The classical equations of motion are obtained from Hamiltonian (9),

$$q(t) = \sqrt{2I} \sin[\beta + \omega(I)t], \quad (16)$$

$$p(t) = \sqrt{2I} \cos[\beta + \omega(I)t], \quad (17)$$

with

$$\omega(I) = \frac{\partial H}{\partial I} = 2\gamma I. \quad (18)$$

Both the action I—a constant of motion—and β are determined by the initial conditions. The trajectories contributing to the Van Vleck propagator are the solutions of the following boundary problem:

$$q'' = \sqrt{2I} \sin[\beta + \omega(I)t], \quad (19)$$

$$q' = \sqrt{2I} \sin(\beta), \quad (20)$$

for a given time t.

Among all trajectories that satisfy the equations above, only a small subset will be relevant to the autocorrelation function. The reason is that the initial wave packet is localized on a phase-space region of radius $\mathcal{O}(\sqrt{\hbar})$, meaning that the important trajectories are only those having end points (q'', p'') and (q', p') in a region of radius $\mathcal{O}(\sqrt{\hbar})$ around the center of the wave packet.

We shall consider, for convenience (but without loss of generality), an initial wave packet corresponding to a coherent state $|\alpha_0\rangle$ located on the p axis, i.e., $\alpha_0 = ip_0/\sqrt{2\hbar}$, whose wave function is

$$\psi_0(q) = (\pi\hbar)^{-1/4} e^{-q^2/2\hbar} e^{ip_0 q/\hbar}. \quad (21)$$

In this case, we can assume that both q'' and q' are small $[\mathcal{O}(\sqrt{\hbar})]$ and resort to Taylor expansions around $(q_0 = 0, p_0)$.

We can get a good idea of the structure of the set of trajectories that we need by analyzing the particular case $q''=q'=0$. From Eqs. (19) and (20) we obtain a set of periodic trajectories, labeled by the winding number k, the corresponding actions being

$$I_k = \frac{p_k^2}{2} = \frac{k\pi}{\gamma t}. \tag{22}$$

The relevant values of k are those satisfying

$$I_k \approx I_0 \equiv \frac{p_0^2}{2}, \tag{23}$$

i.e.,

$$k \approx k_0 \equiv \frac{p_0^2 \gamma t}{2\pi}. \tag{24}$$

For simplicity we ignore $k=0$ trajectories, which would require a special treatment. This means that our calculation is not valid for times of the order or smaller than T_1, where T_1 is the period of the classical motion of the centroid of the wave packet:

$$T_1 = \frac{2\pi}{\omega_0} \equiv \frac{2\pi}{2\gamma I_0} = \frac{\pi}{\gamma I_0}. \tag{25}$$

(This is not a problem as we are interested in long times.) The number of trajectories that contribute at $t \approx kT_1$ is of the order of $\sqrt{k}$ (see Sec. III C). The properties of these periodic trajectories are easily calculated:

$$\mu_k^{(0)} = 2k, \tag{26}$$

$$S_k^{(0)} = 2k\pi I_k - H(I_k)t = \frac{\pi^2 k^2}{\gamma t}, \tag{27}$$

$$A_k^{(0)} = \frac{1}{\sqrt{4I_k \gamma t}}. \tag{28}$$

In the general case, when q'' and/or q' are not strictly zero, even if the corresponding trajectories are not periodic any more, they can be put into one-to-one correspondence with the periodic ones. Accordingly, the actions and amplitudes can be calculated as Taylor expansions in q'' and q' around the periodic solutions. (The Maslov indices do not change, as they just count twice the number of turns.)

We shall approximate the actions S_k to second order in (q'',q') and the amplitudes A_k will be kept at zeroth order [5,7]. So, we need to calculate first and second derivatives of S_k with respect to q'' and q' and evaluate them at $(q''=0,q'=0,t)$. The results are

$$\frac{\partial S_k}{\partial q''} = -\frac{\partial S_k}{\partial q'} = p_k, \tag{29}$$

$$\frac{\partial S_k^2}{\partial q''^2} = \frac{\partial S_k^2}{\partial q'^2} = -\frac{\partial S_k^2}{\partial q' \, \partial q''} = \frac{1}{4I_k \gamma t}. \tag{30}$$

Thus, we arrive at
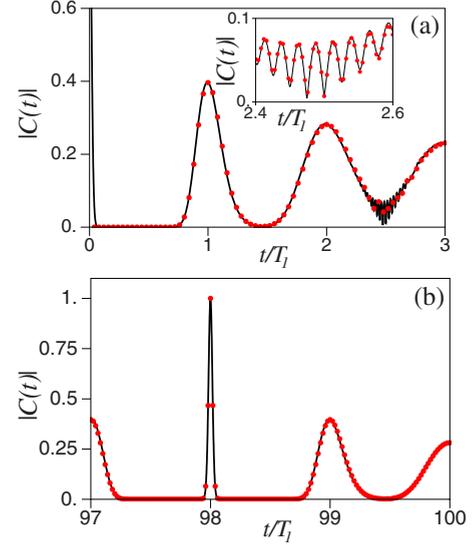
FIG. 2. (Color online) Absolute value of the autocorrelation function vs time, in units of the classical period T_1. Line: exact; dots: semiclassical approximation. We set $m, \omega, \hbar, \gamma = 1$, $p_0 = 14$. (a) Short times. Inset: blowup of the region where the first interference effects appear. (b) Times around the second revival ($t \approx 2T_2$).

$$S_k \approx \frac{\pi^2 k^2}{\gamma t} + \sqrt{\frac{2\pi k}{\gamma t}}(q''-q') + \frac{(q''-q')^2}{8k\pi}, \tag{31}$$

$$A_k \approx A_k^{(0)} = \frac{1}{\sqrt{4I_k \gamma t}}. \tag{32}$$

The final steps in the calculation of the semiclassical correlation function are: (i) substitute the expressions above into Van Vleck propagator (11), (ii) insert the resulting propagator into the definition of correlation function (15), (iii) calculate the Gaussian integrals. In this way we obtain:

$$C_2(t) \approx \frac{e^{-i\pi/4}}{\sqrt{2\pi}} \sum_{k=1}^{\infty} e^{i\pi^2 k^2/\gamma\hbar t} e^{-ik\pi} \frac{e^{-(p_k - p_0)^2/a_k\hbar}}{\sqrt{ka_k}}. \tag{33}$$

with

$$a_k = 1 - \frac{i}{2k\pi}, \tag{34}$$

and $p_k = \sqrt{2k\pi/\gamma t}$.

Equation (33) gives the semiclassical correlation function obtained from Van Vleck's propagator and perturbation analysis around periodic orbits; it is a well behaved sum that can, in principle, be calculated for any t and compared with the exact result. The domain of validity is $t \gtrsim T_1$. Now we proceed to numerical comparisons, postponing analytical considerations to Sec. III C.

In Fig. 2, we display semiclassical and exact correlation functions in two time windows, one for short times [panel (a)], the other for times around the second revival [panel (b)]. Except for the initial correlation peak ($t \approx 0$), where the semiclassical approximation was expected to fail, the agree-

ment is excellent. Remarkably, the peak that is lost at $t \approx 0$, it perfectly resurges at $t \approx 2T_2$ (and at other revival times–graphics not shown).

B. Van Vleck wave function

There is a straightforward test for the wave functions generated by the Van Vleck approach: If, instead of doing both the integrals defining the correlation function in Eq. (15), we calculate only the first one, over q', we obtain a Van Vleck wave function $\psi(q'')$. First of all, this semiclassical wave function can be tested only in a small interval around $q''=0$ (because of the approximations we did in calculating the Van Vleck propagator). Moreover, this calculation omits the contributions arising from trajectories that arrive at q'' in time t *with negative momentum*. So, we expect the approximation to work well only at times where the (Wigner function of the) evolved state does not have negative momentum components around $q''=0$. Such a situation arises, for instance, at revival times, when the initial wave packets are exactly reconstructed.

Another cases that can be described in terms of periodic orbits are fractional revivals such as that at $t=T_2/3$ (see middle panel of Fig. 1), when the wave packet is a superposition of three coherent states with phases $\arg(\alpha) = \pi/2, 2\pi/3, 4\pi/3$. In this case one has:

$$|\psi(t)\rangle = e^{-i\pi/12}c_0|\alpha_0\rangle + \dots, \tag{35}$$

where

$$c_0 = \frac{2 + e^{-2\pi i/3}}{3}, \tag{36}$$

and the ellipsis stand for the other two coherent states.

Figures 3(a) and 3(b) shows that indeed the Van Vleck scheme which only uses periodic orbits reproduces the exact wave functions almost perfectly at times $t=T_2$ and $t=T_2/3$.

In order to calculate the wave function at an arbitrary time (but not too short), we must also take into account the contributions of the family of trajectories that, starting at q', arrive at q'' in time t with negative momentum. As done before, we Taylor-expand actions and amplitudes around the main family ($q''=0, q'=0$). These are "half-periodic" trajectories, i.e., their frequencies satisfy $\omega_k t = 2\pi(k-1/2)$, for $k \geq 1$. We skip the details and just show the final results:

$$S_k \approx \frac{\pi^2 k^2}{\gamma t} - \sqrt{\frac{2\pi k}{\gamma t}}(q'' + q') + \frac{(q'' + q')^2}{8k\pi}, \tag{37}$$

$$A_k \approx \frac{1}{\sqrt{4I_k\gamma t}}, \tag{38}$$

$$\mu_k = 2k - 1. \tag{39}$$

Adding the contributions of the family above to that of the periodic trajectories we obtain a semiclassical wave function valid for arbitrary times. Figure 3 (bottom panel) compares semiclassical and exact wave functions at a time when the state is completely delocalized in phase space (rightmost
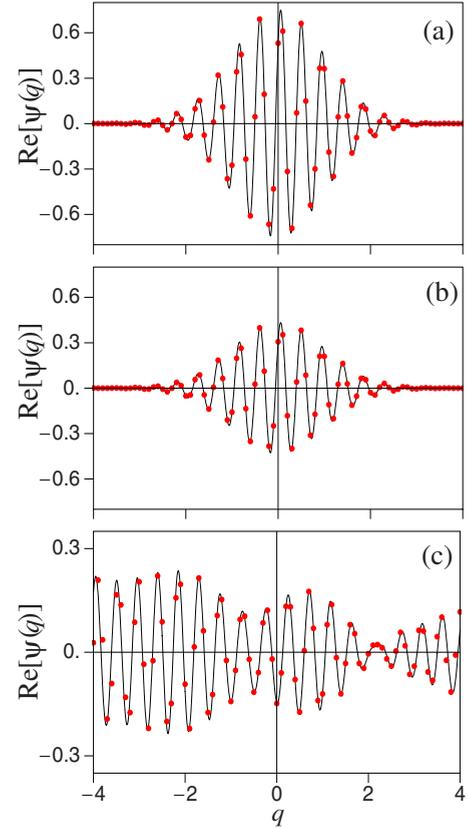
FIG. 3. (Color online) Real part of the wave function $\psi(q)$ vs q at some selected times. Line: exact; dots: Van Vleck. Similar agreement is observed for the imaginary part. We used $m=\omega=\hbar=\gamma=1$, $p_0=14$. (a) At the first revival time. (b) At the fractional revival time $t=T_2/3$. (c) At $t=T_2/2.385\,67$, when the wave function is completely delocalized.

panel in Fig. 1). Again, the semiclassical approximation performs remarkably well for small enough values of q. Not unexpectedly, for $|q| \approx 3$ some small deviations start to show up, and keep growing with increasing $|q|$.

C. Analytical comparisons

The striking accuracy of the semiclassical approximations verified in the previous sections, together with the relative simplicity of the expressions involved, suggests that it should be possible to give an analytical explanation of the approximate quantum-semiclassical equivalence. In the following we show analytically that the error committed in the semiclassical autocorrelation function is really very small and, what is especially important, independent of time. (A similar analysis could in principle be carried out for wave functions but will not be attempted here.)

When comparing semiclassical (33) and exact (7) correlation functions we immediately see a fundamental difference: time appears in a different way in both expressions. While the quantum expression is a Fourier series, i.e., a sum of plane waves (in t), the semiclassical correlation is a sum of wave packets, or wave trains. The tool that switches between wave trains and plane waves is Poisson transformation

[19]. But before applying Poisson transformation to, say, the quantum correlation function let us introduce a small simplification.

1. Quantum correlation function

For large $|\alpha_0|^2$ one can approximate the Poisson distribution by a Gaussian [19]:

$$e^{-|\alpha_0|^2}\frac{|\alpha_0|^{2n}}{n!} \approx \frac{1}{\sqrt{2\pi\nu}}e^{-(n-\nu+1/2)^2/2\nu}, \qquad (40)$$

where $\nu=|\alpha_0|^2$. With this approximation the exact autocorrelation can be written in terms of the Jacobi theta function [21]

$$\vartheta_3(z|\tau) = \sum_{n=-\infty}^{\infty} e^{\pi i n^2 \tau + 2inz}. \qquad (41)$$

In fact, after the substitution Poisson-to-Gaussian in Eq. (7), we extend the lower limit of the summation to $-\infty$, obtaining

$$C_1(t) \approx \frac{1}{\sqrt{2\pi\nu}}e^{-(\nu-1/2)^2/2\nu}e^{-i\gamma\hbar t/4}\vartheta_3(z_1|\tau_1), \qquad (42)$$

where

$$z_1 = \frac{1}{2i}\left(1 - \frac{1}{2\nu} - i\gamma\hbar t\right), \qquad (43)$$

$$\tau_1 = \frac{1}{\pi i}\left(-\frac{1}{2\nu} - i\gamma\hbar t\right). \qquad (44)$$

Expressing $C_1(t)$ in terms of ϑ_3 brings in several benefits. First, formulas become more compact and can be calculated quickly and efficiently using standard softwares, e.g., Mathematica [22], where ϑ_3 is a built-in function. Second, Poisson transforming the theta function is equivalent to using the *functional equation*

$$\vartheta_3(z|\tau) = (-i\tau)^{-1/2}e^{z^2/\pi i \tau}\vartheta_3\left(\frac{z}{\tau}\middle| -\frac{1}{\tau}\right), \qquad (45)$$

where $(-i\tau)^{-1/2}$ is to be interpreted by the convention $|\arg(-i\tau)| < \pi/2$ [21]. (This equation has already been used by Wang and Heller in their semiclassical study of the square well [15].)

Now we use the functional equation but restricting ourselves to times longer than the period T_1, i.e., $\gamma\hbar t \gg \nu$. So,

$$\frac{z_1}{\tau_1} \equiv z_1' = \frac{\pi}{2} + \frac{i\pi}{2\gamma\hbar t} + \cdots, \qquad (46)$$

$$-\frac{1}{\tau_1} \equiv \tau_1' = \frac{\pi}{\gamma\hbar t} + \frac{i\pi}{2\nu\gamma^2\hbar^2 t^2} + \cdots, \qquad (47)$$

$$\frac{z_1^2}{\pi i \tau_1} = \frac{i\gamma\hbar t}{4} - \frac{1}{2} + \frac{1}{8\nu} + \cdots, \qquad (48)$$
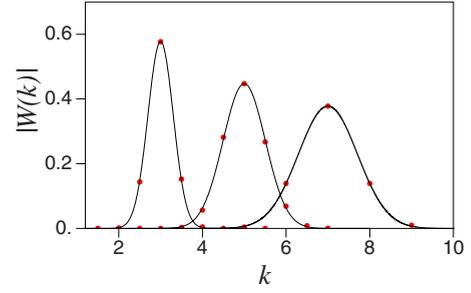
FIG. 4. (Color online) Orbit weight function for times $t/T_1 = 3, 5, 7$ (from left to right, respectively). Lines: Gaussian approximation, with k a continuous variable. Dots: absolute value of exact weight. Parameters are $m, \omega, \gamma, \hbar = 1$, $p_0 = 14$.

$$(-i\tau_1)^{-1/2} = e^{-i\pi/4}\sqrt{\frac{\pi}{\gamma\hbar t}} + \cdots. \qquad (49)$$

In this way we arrive at an approximate expression for the quantum correlation function which has a semiclassical appearance:

$$C_1(t) \approx \frac{e^{-\nu/2}}{\sqrt{2\nu\gamma\hbar t}}e^{-i\pi/4}\vartheta_3(z_1'|\tau_1'). \qquad (50)$$

Before comparing this expression with the semiclassical one we shall do some manipulations of the semiclassical formula.

2. Van Vleck correlation function

The semiclassical correlation function is written as a sum over periodic orbits. Each orbit is weighted by the exponential function:

$$W(k) \equiv \frac{e^{-(p_k - p_0)^2/a_k\hbar}}{\sqrt{ka_k}}. \qquad (51)$$

Recall that this function depends on time through p_k Eq. (22). For long times (large k) we can set $a_k \approx 1$. Thus $W(k)$ becomes a real function, which can be well approximated by a Gaussian.

We show in Fig. 4 some plots of the exact $W(k)$ [Eq. (51)] for typical values of the parameters together with the simplest Gaussian approximation obtained by setting $k=k_0$, $a_k=1$ in the denominator, and linear expanding p_k around $k=k_0$, i.e.,

$$W(k) \approx \frac{e^{-\pi(k-k_0)^2/2k_0\gamma\hbar t}}{\sqrt{k_0}}. \qquad (52)$$

It is verified that the Gaussian approximation is already very good for the small values of k considered.

The remarkable fact is that if we substitute the approximate weight function (52) into the semiclassical correlation function (33) we obtain the approximate quantum correlation function (50). This concludes the analytical comparison of quantum and semiclassical correlation functions. Even if we have not exhibited an explicit strict bound for the error of the semiclassical approximation, we provided strong evidence that the difference between the exact and semiclassical cor-

relation functions is bounded for arbitrarily long times, the bound decreasing with increasing $|\alpha_0|$. (Note that this is much stronger than the general statement that the semiclassical approximation is a leading term of the asymptotic expansion of the exact quantum dynamics, which presupposes the limit of $\hbar$ going to zero for a fixed time.)

IV. TDWKB APPROACH

It was recently shown that when the underlying classical dynamics of a system is chaotic the evolution of a Gaussian wave packet can be described by the standard TDWKB method [8]. The reason is that, in semiclassical regimes, after some short time the Gaussian wave packet stretches over a classical length $\sim \hbar^0$. Thus, it becomes a primitive WKB state,

$$\psi_0(q) = A_0(q)\exp[iS_0(q)/\hbar], \qquad (53)$$

supported by the Lagrangian manifold defined by

$$p = dS_0/dq, \qquad (54)$$

and where the amplitude $A_0(q)$ and the phase $S_0(q)$ are smooth function on the quantum scale. From then on the wave function evolves according to the TDWKB recipe,

$$\psi_t(q) \approx \sum_\nu A_t^{(\nu)}(q)\exp[iS_t^{(\nu)}(q)/\hbar - i\mu_\nu\pi/2], \qquad (55)$$

where ν labels the different branches of the Lagrangian manifold obtained by evolving classically the initial manifold Eq. (54).

In chaotic systems the applicability of TDWKB to wave packets is guaranteed by the exponentially fast stretching of phase space [8]. We show here that the same scheme can be applied in the case of *integrable nonlinear* systems, where the stretching is linear in time.

For the present analysis we found more convenient to make a slight modification of the Hamiltonian of previous sections,

$$\hat{H} = \gamma\hbar^2(\hat{n} - n_0)^2. \qquad (56)$$

The corresponding classical Hamiltonian is

$$H(q,p) = \gamma(I - I_0)^2. \qquad (57)$$

This is equivalent to working with the Hamiltonian Eq. (3) but in the interaction representation, with a free evolution given by the harmonic oscillator $\hat{H}_0 = \hbar\omega'\hat{n} + C$ [with $\omega' = 2\gamma\hbar(n_0 + 1/2)$ and C an appropriate constant)]. Thus, we eliminate the rotation dynamics of the wave packet, while preserving the nonlinear squeezing. This choice simplifies the determination of the initial WKB manifold Eq. (54), which now remains almost stationary; otherwise it would rotate, forcing us to change representation from time to time to avoid caustics. Switching to the interaction representation does not affect the semiclassical accuracy of the calculation, because the transformation generated by $\hat{H}_0$ is semiclassically exact [23].
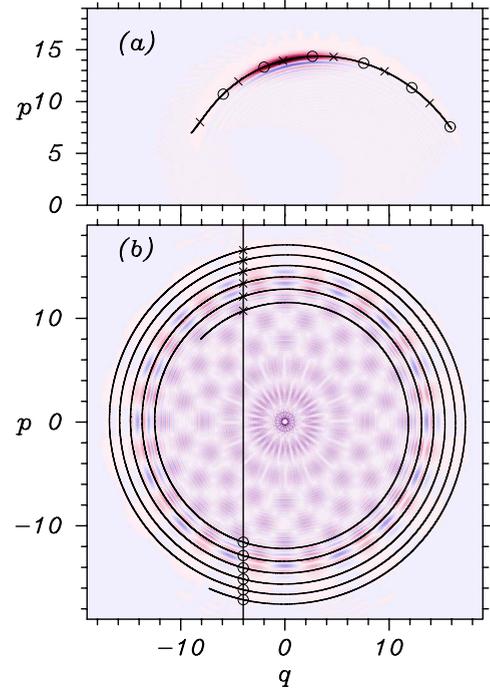
FIG. 5. (a) (Color online) Wigner function of the evolved initial coherent state, centered at the point $(q_0, p_0) = (0, 14)$, for a time $t = T_2/320$ (T_2 the revival time). The superimposed black line is the initial Lagrangian manifold. (b) Wigner function of the same initial coherent state at $t = T_2/16$. The spiraling black line is the classical evolved manifold that supports the WKB state. Parameters are $m, \gamma, \hbar = 1$. See text for explanation of the meaning of crosses and circles.

The centroid (q_0, p_0) of the initial wave packet will be chosen in such a way that $I_0 = \hbar(n_0 + 1/2) = (q_0 + p_0)/2$. The numerical implementation of the TDWKB recipe [8] requires the determination of the initial manifold through Eq. (54). The initial action $S_0(q)$ is extracted from the phase of the exact wave function propagated up to some short time t_i. The only condition this time must satisfy is that the exact wave function must be described to good accuracy by a primitive WKB state, i.e., Eq. (53) with $A(q)$ and $S(q)$ smooth on the quantum scale.

Our choice of the initial manifold is showed in Fig. 5(a). Using the classical equations of motion we evolve this initial manifold up to the desired final time [see Fig. 5(b)]. In order to calculate the WKB wave function $\psi_t(q)$ we have to determine the classical trajectories corresponding to each term in the sum in Eq. (55). Those are the trajectories that at times t_i have initial conditions $(q_j^{(i)}, p_j^{(i)})$ on the initial manifold, and at time t reach the final manifold at the points $(q_j^{(f)}, p_j^{(f)})$, where $q_j^{(f)} = q$ for all values of j. For example, in Fig. 5 we show with crosses in panel (a) the initial conditions of the trajectories that end at points $(q_j^{(f)} = q, p_j^{(f)})$ with positive momentum [panel (b)], and with circles the trajectories that end with a negative momentum. The classical action for these trajectories can be calculated analytically for the Hamiltonian in Eq. (57),

$$S_t^{(j)} = S_0 + \int_{t_i}^{t} (p\dot{q} - H)dt$$

$$= S_0 + \frac{1}{2}(p_j^{(f)}q_j^{(f)} - p_j^{(i)}q_j^{(i)}) + (\omega(I_j)I_j - H_j)\Delta t, \quad (58)$$

where $\omega(I_j) \equiv 2\gamma(I_j - I_0)$, $H_j \equiv \gamma(I_j - I_0)^2$ and $\Delta t \equiv t - t_i$. The Maslov index μ in Eq. (55) equals $+/-$ the number of turning points along a clockwise/counterclockwise trajectory [9]. The amplitudes $A_t^{(j)}$ in Eq. (55) are calculated from the continuity equation

$$A_t^{(j)}(q_j^{(f)} = q) = A_0(q_j^{(i)})\left|\frac{dq_i}{dq_f}\right|^{1/2}, \quad (59)$$

where $A_0(q_j^{(i)})$ is the amplitude of the primitive WKB wave function supported by the initial manifold. The factor $|dq_i/dq_f|$ is determined by evolving numerically a nearby trajectory.

Note that the relatively hard part of this numerical method is the calculation of the points $(q_j^{(i)}, p_j^{(i)})$ and $(q_j^{(f)} = q, p_j^{(f)})$ in the initial and the final Lagrangian manifolds, respectively. This can be done in a systematic way defining a parameter s running along the initial manifold and calculating the points $(q_j^{(f)}, p_j^{(f)})$ as intersections of the trajectories, with parameter s and fixed elapsed time t, with the phase-space vertical line $q = q^{(f)}$, in a way resembling a Poincaré section map.

In Fig. 6 we compare the exact wave function of an initially coherent state with the TDWKB wave function for $t = 4T_2$ in panel (a) and for a generic time in panel (b) [when the Wigner function is nonlocalized, similar to the wave function in the rightmost panel of Fig. 1]. In panel (a) we see that the agreement is very good for all values of q, with small errors for $|q| > 1.8$. For multiples of the revival time, $t = mT_2$, the number of classical trajectories needed to build up the TDWKB wave function grows like $\propto 90 \ m$. Nevertheless, the numerical errors seem to be almost constant. Like in the Van Vleck approach of Sec. III, at multiples of the revival time only classical trajectories with positive final momenta contribute.

In Fig. 6(b) we show the TDWKB approximation in the generic case, where trajectories with final negative momenta also contribute. In this example, the exact wave function spreads also over the regions $-17 < q < -11$ and $11 < q < 17$, where the final manifold crosses several times the axis $p = 0$. These points are caustics of the TDWKB approximation, where the amplitude in Eq. (59) diverges. Thus, each time the contributing trajectories has a null final momentum, the TDWKB approximation breaks down. This is clearly seen in Fig. 6(b). The proper treatment of the WKB function in this region requires more sophisticated approximations. For our present purposes, it is enough to verify that for $|q| < 10$, where there are no caustic points, the agreement is excellent.

V. CONCLUDING REMARKS

Quantum revival is a subtle phenomenon where interference plays a crucial role. We studied revivals in the quartic oscillator from a semiclassical perspective. Among various

(a)

(b)
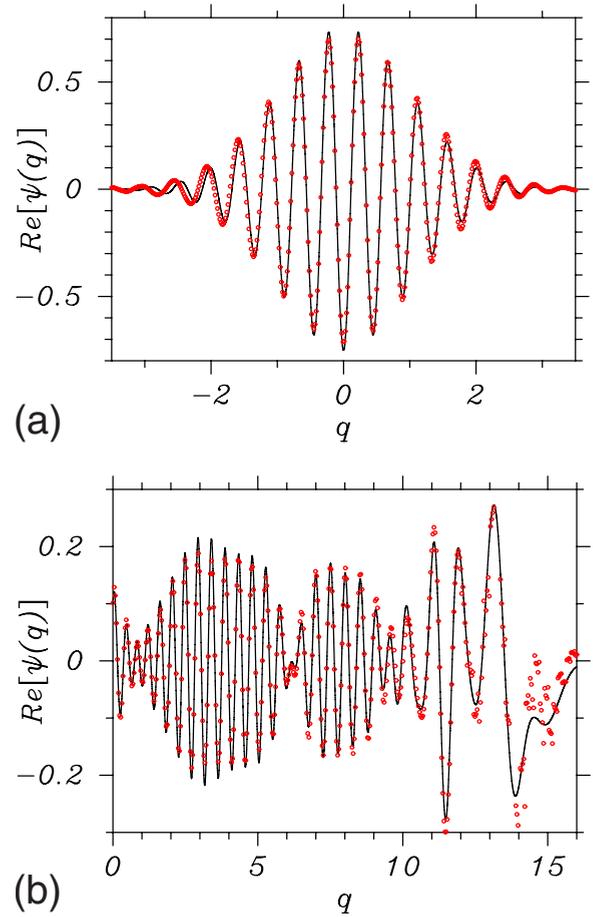
FIG. 6. (Color online) Real part of the evolved wave function of an initially coherent state centered at the point $(q_0, p_0) = (0, 14)$ evolved with the Hamiltonian of Eq. (56). The full line is the exact wave function and the circles correspond to the TDWKB approximation. (a) For $t = 4T_2$ (T_2 is the revival time); (b) For $T_2/2.385\,67$. Similar agreement is observed for $q < 0$ and for the imaginary parts. Parameters are $m, \gamma, \hbar = 1$.

semiclassical theories existing in the literature we chose two of most basic and popular: Van Vleck propagation and time-dependent WKB. In both cases the results were impressive: quantum dynamics—in particular, revivals—can be semiclassically described with great accuracy.

In the TDWKB approach, we computed the wave function numerically for times beyond the first revivals. Excluding an initial stage (where standard WKB fails), the classical skeleton of the wave function appeared to be a spiraling manifold. Thus, we have exhibited another successful test of the TDWKB scheme for the propagation of wave packets [8]—in this occasion for the long-time dynamics of an integrable system. However, at present, we cannot assess analytically how far the agreement will extend. In order to do this one should integrate the present scheme with a theory capable of describing the short time dynamics. The natural tool is *complex* TDWKB which uses manifolds in the complexified phase space [24]. Then one should prove that, provided the dynamics is stretching, the complex manifold describing a coherent state eventually decays into a real manifold [such as that shown in Fig. 5(a)].

Like in some previous studies [6,7], we obtained an expression for the autocorrelation function as a sum over classical trajectories, all the ingredients being given in closed form. Furthermore, we showed analytically that the Van Vleck correlation function and the exact one are essentially equal. The key step was to use the Poisson transformation, which reshapes a semiclassical correlation function into a quantum-looking one, or vice versa. Similar analyses may be possible both for the Coulomb potential [6,7] and the Morse oscillator [15] (the latter is simpler, in principle, because its spectrum is quadratic in the quantum number [25]).

The system under study, the quartic oscillator, is special, even among integrable systems, in that its Hamiltonian is a (quadratic) function of the action variable. Thus, for instance, stationary WKB theory gives the exact energy levels for this system. We have provided analytical and numerical evidence showing that the semiclassical *time-dependent* schemes considered in this paper are also "exact." It remains to ascertain if these considerations extend to more general $H(I)$ Hamiltonians, e.g., of the polinomial type.

Concerning the work by Novaes [16], who studied the quartic oscillator by using the semiclassical coherent-state representation of the propagator, it is likely, in the light of our results, that it should be possible to identify the relevant subset of complex trajectories which contribute to the autocorrelation function at long times.

Even if the methods presented here can in principle be generalized to systems with several degrees of freedom, it is clear that search of specific trajectories ("root searching") will be extremely expensive at higher dimensions. One way to avoid this problem is to map the present methods into IVR schemes, thus substituting root searching by integration over initial conditions [10]. The efficient implementation of this strategy is currently under investigation.

[1] V. P. Maslov and M. V. Fedoriuk, *Semiclassical Approximations in Quantum Mechanics* (Reidel, Dordrecht, 1981).

[2] M. Brack and R. K. Bhaduri, *Semiclassical Physics, Frontiers in Physics, 96* (Westview, Boulder, CO, 2003).

[3] J. H. Van Vleck, Proc. Natl. Acad. Sci. U.S.A. **14**, 178 (1928).

[4] M. C. Gutzwiller, J. Math. Phys. **8**, 1979 (1967).

[5] S. Tomsovic and E. J. Heller, Phys. Rev. Lett. **67**, 664 (1991); Phys. Rev. E **47**, 282 (1993).

[6] M. Mallalieu and C. R. Stroud, Jr., Phys. Rev. A **49**, 2329 (1994).

[7] I. M. Suarez Barnes, M. Nauenberg, M. Nockleby, and S. Tomsovic, Phys. Rev. Lett. **71**, 1961 (1993); J. Phys. A **27**, 3299 (1994).

[8] R. N. P. Maia, F. Nicacio, F. Toscano, and R. O. Vallejos, Phys. Rev. Lett. **100**, 184102 (2008).

[9] R. G. Littlejohn, J. Stat. Phys. **68**, 7 (1992).

[10] W. H. Miller, J. Phys. Chem. A **105**, 2942 (2001).

[11] R. W. Robinett, Phys. Rep. **392**, 1 (2004).

[12] J. A. Yeazell, M. Mallalieu, and C. R. Stroud, Jr., Phys. Rev. Lett. **64**, 2007 (1990); M. J. J. Vrakking, D. M. Villeneuve, and A. Stolow, Phys. Rev. A **54**, R37 (1996); G. Rempe, H. Walther, and N. Klein, Phys. Rev. Lett. **58**, 353 (1987); F. Diedrich, J. Krause, G. Rempe, M. O. Scully, and H. Walther, IEEE J. Quantum Electron. **24**, 1314 (1988).

[13] B. Yurke and D. Stoler, Phys. Rev. Lett. **57**, 13 (1986); Ts. Gantsong and R. Tanaś, Quantum Opt. **3**, 33 (1991); K. Tara, G. S. Agarwal, and S. Chaturvedi, Phys. Rev. A **47**, 5024 (1993).

[14] S. L. Braunstein and P. van Look, Rev. Mod. Phys. **77**, 513 (2005).

[15] Z. Wang and E. J. Heller, J. Phys. A: Math. Theor. **42**, 285304 (2009).

[16] M. Novaes, J. Math. Phys. **46**, 102102 (2005).

[17] C. Cohen-Tannoudji, B. Diu, and F. Laloë, *Quantum Mechanics* (Wiley, New York, 1977), Vol. 1.

[18] D. F. Walls and G. Milburn, *Quantum Optics* (Springer, Berlin, 1995).

[19] W. P. Schleich, *Quantum Optics in Phase Space* (Wiley-VCH, Berlin, 2001).

[20] A. M. Ozorio de Almeida, Phys. Rep. **295**, 265 (1998).

[21] E. T. Whittaker and G. N. Watson, *A Course of Modern Analysis* (Cambridge University Press, Cambridge, 1927); D. Mumford, *Tata Lectures on Theta I* (Birkhäuser, Boston, 1983).

[22] E. W. Weisstein, Jacobi Theta Functions, From MathWorld—A Wolfram Web Resource (http://mathworld.wolfram.com/JacobiThetaFunctions.html).

[23] R. G. Littlejohn, Phys. Rep. **138**, 193 (1986).

[24] D. Huber, E. J. Heller, and R. G. Littlejohn, J. Chem. Phys. **89**, 2003 (1988); V. P. Maslov, *The Complex WKB Method for Nonlinear Equations I* (Birkhäuser, Basel, 1994); M. A. M. de Aguiar, M. Baranger, L. Jaubert, F. Parisio, and A. D. Ribeiro, J. Phys. A **38**, 4645 (2005).

[25] M. S. Child, *Semiclassical Mechanics with Molecular Applications* (Oxford University Press, Oxford, 1991).